Probing Cold Dense Nuclear Matter

R. Subedi,[1] R. Shneor,[2] P. Monaghan,[3] B. D. Anderson,[1] K. Aniol,[4] J. Annand,[5] J. Arrington,[6] H. Benaoum,[7,8] F. Benmokhtar,[9] W. Boeglin,[10] J.-P. Chen,[11] Seonho Choi,[12] E. Cisbani,[13] B. Craver,[14] S. Frullani,[13] F. Garibaldi,[13] S. Gilad,[3] R. Gilman,[11,15] O. Glamazdin,[16] J.-O. Hansen,[11] D. W. Higinbotham,[11]* T. Holmstrom,[17] H. Ibrahim,[18] R. Igarashi,[19] C. W. de Jager,[11] E. Jans,[20] X. Jiang,[15] L. J. Kaufman,[9,21] A. Kelleher,[17] A. Kolarkar,[22] G. Kumbartzki,[15] J. J. LeRose,[11] R. Lindgren,[14] N. Liyanage,[14] D. J. Margaziotis,[4] P. Markowitz,[10] S. Marrone,[23] M. Mazouz,[24] D. Meekins,[11] R. Michaels,[11] B. Moffit,[17] C. F. Perdrisat,[17] E. Piasetzky,[2] M. Potokar,[25] V. Punjabi,[26] Y. Qiang,[3] J. Reinhold,[10] G. Ron,[2] G. Rosner,[27] A. Saha,[11] B. Sawatzky,[14,28] A. Shahinyan,[29] S. Širca,[25,30] K. Slifer,[14] P. Solvignon,[28] V. Sulkosky,[17] G. M. Urciuoli,[13] E. Voutier,[24] J. W. Watson,[1] L. B. Weinstein,[18] B. Wojtsekhowski,[11] S. Wood,[11] X.-C. Zheng,[3,6,14] L. Zhu[31]

The protons and neutrons in a nucleus can form strongly correlated nucleon pairs. Scattering experiments, in which a proton is knocked out of the nucleus with high-momentum transfer and high missing momentum, show that in carbon-12 the neutron-proton pairs are nearly 20 times as prevalent as proton-proton pairs and, by inference, neutron-neutron pairs. This difference between the types of pairs is due to the nature of the strong force and has implications for understanding cold dense nuclear systems such as neutron stars.

Nuclei are composed of bound protons (p) and neutrons (n), referred to collectively as nucleons (N). A standard model of the nucleus since the 1950s has been the nuclear shell model, in which neutrons and protons move independently in well-defined quantum orbits in the average nuclear field created by their mutually attractive interactions. In the 1980s and 1990s, proton-removal experiments using electron beams with energies of several hundred megaelectron volts showed that only 60 to 70% of the protons participate in this type of independent particle motion in nuclear valence states (*1*, *2*). At the time, it was assumed that this low occupancy was caused by correlated pairs of nucleons within the nucleus. The existence of nucleon pairs that are correlated at distances of several femtometers, known as long-range correlations, has been established (*3*), but these accounted for less than half of the predicted correlated nucleon pairs. Recent high-momentum transfer measurements (*4*–*12*) have shown that nucleons in nuclear ground states can form pairs with large relative momentum and small center-of-mass (CM) momentum due to the short-range (scalar and tensor) components of the nucleon-nucleon interaction. These pairs are referred to as short-range correlated (SRC) pairs. The study of these SRC pairs allows access to cold dense nuclear matter, such as that found in a neutron star.

Experimentally, a high-momentum probe can knock a proton out of a nucleus, leaving the rest of the system nearly unaffected. If, on the other hand, the proton being struck is part of an SRC pair, the high relative momentum in the pair would cause the correlated nucleon to recoil and be ejected as well (Fig. 1). High-momentum knockout by both high-energy protons (*8*–*10*) and high-energy electrons (*12*) has shown, for kinematics far from particle-production resonances, that when a proton with high missing momentum is removed from the ^{12}C nucleus, the momentum is predominantly balanced by a single recoiling nucleon. This is consistent with the theoretical description that large nucleon momenta in the nucleus are predominantly caused by SRC pairing (*13*). This effect has also been shown when inclusive incident electron, scattered electron (e,e') data were used (*4*, *5*, *14*), although that type of measurement is not sensitive to the type of SRC pair. Here we identify the relative abundance of p-n and p-p SRC pairs in ^{12}C nuclei.

We performed our experiment in Hall A of the Thomas Jefferson National Accelerator Facility (JLab), using an incident electron beam of 4.627 GeV with a beam current between 5 and 40 μA. The beam was incident on a 0.25-mm-thick pure ^{12}C sheet rotated 70° to the beam line to minimize the material through which the recoiling protons passed. We used two high-resolution spectrometers (HRS) (*15*) to define proton-knockout events for ^{12}C(e,e'p). The left HRS detected scattered electrons at a central scattering angle (momentum) of 19.5° (3.724 GeV/c). These values correspond to the quasi-free knockout of a single proton with transferred three-momentum q = 1.65 GeV/c, transferred energy ω = 0.865 GeV, $Q^2 = q^2 - (\omega/c)^2 = 2(\mathrm{GeV}/c)^2$ (where Q^2 is the four-momentum, squared), and Bjorken scaling parameter $x_B = Q^2/2m\omega = 1.2$, where m is the mass of the proton. The right HRS detected knocked-out protons at three different values for the central angle (momentum): 40.1° (1.45 GeV/c), 35.8° (1.42 GeV/c), and 32.0° (1.36 GeV/c).

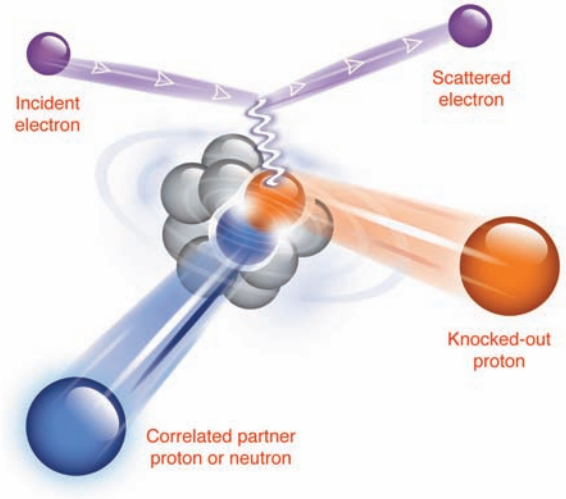

Fig. 1. Illustration of the ^{12}C(e,e'pN) reaction. The incident electron beam couples to a nucleon-nucleon pair via a virtual photon. In the final state, the scattered electron is detected along with the two nucleons that are ejected from the nucleus. Typical nuclear density is about 0.16 nucleons/fm^3, whereas for pairs the local density is approximately five times larger.

[1]Kent State University, Kent State, OH 44242, USA. [2]Tel Aviv University, Tel Aviv 69978, Israel. [3]Massachusetts Institute of Technology, Cambridge, MA 02139, USA. [4]California State University Los Angeles, Los Angeles, CA 90032, USA. [5]University of Glasgow, Glasgow G12 8QQ, Scotland, UK. [6]Argonne National Laboratory, Argonne, IL 60439, USA. [7]Syracuse University, Syracuse, NY 13244, USA. [8]Prince Mohammad University, Al-Khobar 31952, Saudi Arabia. [9]University of Maryland, College Park, MD 20742, USA. [10]Florida International University, Miami, FL 33199, USA. [11]Thomas Jefferson National Accelerator Facility, Newport News, VA 23606, USA. [12]Seoul National University, Seoul 151-747, Korea. [13]Istituto Nazionale de Fisica Nucleare (INFN), Sezione di Roma, I-00185 Rome, Italy. [14]University of Virginia, Charlottesville, VA 22904, USA. [15]Rutgers, The State University of New Jersey, Piscataway, NJ 08855, USA. [16]Kharkov Institute of Physics and Technology, Kharkov 310108, Ukraine. [17]College of William and Mary, Williamsburg, VA 23187, USA. [18]Old Dominion University, Norfolk, VA 23508, USA. [19]University of Saskatchewan, Saskatoon, Saskatchewan, S7N 5E2 Canada. [20]Nationaal Instituut voor Subatomaire Fysica, Amsterdam, Netherlands. [21]University of Massachusetts Amherst, Amherst, MA 01003, USA. [22]University of Kentucky, Lexington, KY 40506, USA. [23]Dipartimento di Fisica and INFN sezione Bari, Bari, Italy. [24]Laboratoire de Physique Subatomique et de Cosmologie, F-38026 Grenoble, France. [25]Institute "Jožef Stefan," 1000 Ljubljana, Slovenia. [26]Norfolk State University, Norfolk, VA 23504, USA. [27]University of Glasgow, Glasgow G12 8QQ, Scotland, UK. [28]Temple University, Philadelphia, PA 19122, USA. [29]Yerevan Physics Institute, Yerevan 375036, Armenia. [30]Department of Physics, University of Ljubljana, 1000 Ljubljana, Slovenia. [31]University of Illinois at Urbana–Champaign, Urbana, IL 61801, USA.

*To whom correspondence should be addressed. E-mail: doug@jlab.org

These kinematic settings covered (e,e'p) missing momenta, which is the momentum of the undetected particles, in the range from 300 to 600 MeV/c, with overlap between the different settings. For highly correlated pairs, the missing momentum of the (e,e'p) reaction is balanced almost entirely by a single recoiling nucleon, whereas for a typical uncorrelated (e,e'p) event, the missing momentum is balanced by the sum of many recoiling nucleons. In a partonic picture, x_B is the fraction of the nucleon momentum carried by the struck quark. Hence, when $x_B > 1$, the struck quark has more momentum than the entire nucleon, which points to nucleon correlation. To detect correlated recoiling protons, a large acceptance spectrometer ("BigBite") was placed at an angle of 99° to the beam direction and 1.1 m from the target. To detect correlated recoiling neutrons, a neutron array was placed directly behind the BigBite spectrometer at a distance of 6 m from the target. Details of these custom proton and neutron detectors can be found in the supporting online material (*16*).

The electronics for the experiment were set up so that for every ^{12}C(e,e'p) event in the HRS spectrometers, we read out the BigBite and neutron-detector electronics; thus, we could determine the ^{12}C(e,e'pp)/^{12}C(e,e'p) and the ^{12}C(e,e'pn)/^{12}C(e,e'p) ratios. For the ^{12}C(e,e'pp)/^{12}C(e,e'p) ratio, we found that 9.5 ± 2% of the (e,e'p) events had an associated recoiling proton, as reported in (*12*). Taking into account the finite acceptance of the neutron detector [using the same procedure as with the proton detector (*12*)] and the neutron detection efficency, we found that 96 ± 22% of the (e,e'p) events with a missing momentum above 300 MeV/c had a recoiling neutron. This result agrees with a hadron beam measurement of (p,2pn)/(p,2p), in which 92 ± 18% of the (p,2pn) events with a missing momentum above the Fermi momentum of 275 MeV/c were found to have a single recoiling neutron carrying the momentum (*11*).

Because we collected the recoiling proton ^{12}C(e,e'pp) and neutron ^{12}C(e,e'pn) data simultaneously with detection systems covering nearly identical solid angles, we could also directly determine the ratio of ^{12}C(e,e'pn)/^{12}C(e,e'pp). In this scheme, many of the systematic factors needed to compare the rates of the ^{12}C(e,e'pn) and ^{12}C(e,e'pp) reactions canceled out. Correcting only for detector efficiencies, we determined that this ratio was 8.1 ± 2.2. To estimate the effect of final-state interactions (that is, reactions that happen after the initial scattering), we assumed that the attenuations of the recoiling protons and neutrons were almost equal. In this case, the only correction related to final-state interactions of the measured ^{12}C(e,e'pn)/^{12}C(e,e'pp) ratio is due to a single-charge exchange. Because the measured (e,e'pn) rate is about an order of magnitude larger than the (e,e'pp) rate, (e,e'pn) reactions followed by a single-charge exchange [and hence detected as (e,e'pp)] dominated and reduced the measured ^{12}C(e,e'pn)/^{12}C(e,e'pp) ratio. Using the Glauber approximation (*17*), we estimated that this effect was 11%. Taking this into account, the corrected experimental ratio for ^{12}C(e,e'pn)/^{12}C(e,e'pp) was 9.0 ± 2.5.

To deduce the ratio of p-n to p-p SRC pairs in the ground state of ^{12}C, we used the measured ^{12}C(e,e'pn)/^{12}C(e,e'pp) ratio. Because we used (e,e'p) events to search for SRC nucleon pairs, the probability of detecting p-p pairs was twice that of p-n pairs; thus, we conclude that the ratio of p-n/p-p pairs in the ^{12}C ground state is 18 ± 5 (Fig. 2). To get a comprehensive picture of the structure of ^{12}C, we combined the pair faction results with the inclusive ^{12}C(e,e') measurements (*4*, *5*, *14*) and found that approximately 20% of the nucleons in ^{12}C form SRC pairs, consistent with the depletion seen in the spectroscopy experiments (*1*, *2*). As shown in Fig. 3, the combined results indicate that 80% of the nucleons in the ^{12}C nucleus acted independently or as described within the shell model, whereas for the 20% of correlated pairs, 90 ± 10% were in the form of p-n SRC pairs; 5 ± 1.5% were in the form of p-p SRC pairs; and, by isospin symmetry, we inferred that 5 ± 1.5% were in the form of SRC n-n pairs. The dominance of the p-n over p-p SRC pairs is a clear consequence of the nucleon-nucleon tensor force. Calculations of this effect (*18*, *19*) indicate that it is robust and does not depend on the exact parameterization of the nucleon-nucleon force, the type of the nucleus, or the exact ground-state wave function used to describe the nucleons.

If neutron stars consisted only of neutrons, the relatively weak n-n short-range interaction would mean that they could be reasonably well approximated as an ideal Fermi gas, with only perturbative corrections. However, theoretical analysis of neutrino cooling data indicates that neutron stars contain about 5 to 10% protons and electrons in the first central layers (*20*–*22*). The strong p-n short-range interaction reported here suggests that momentum distribution for the protons and neutrons in neutron stars will be substantially different from that characteristic of an ideal Fermi gas. A theoretical calculation that takes into account the p-n correlation effect at relevant neutron star densities and realistic proton concentration shows the correlation effect on the momentum distribution of the protons and the neutrons (*23*). We therefore speculate that the small concentration of protons inside neutron stars might have a disproportionately large effect that needs to be addressed in realistic descriptions of neutron stars.

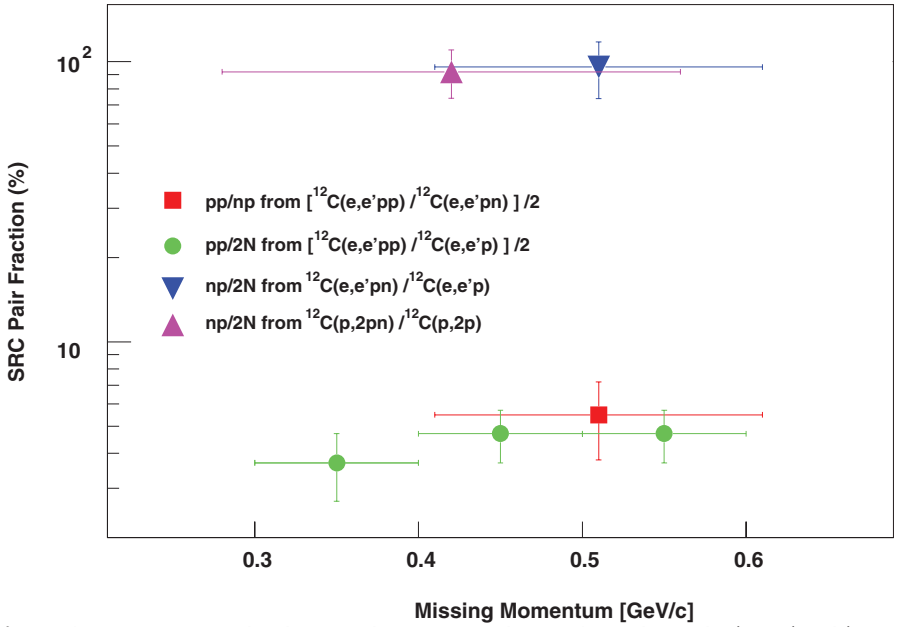

Fig. 2. The fractions of correlated pair combinations in carbon as obtained from the (e,e'pp) and (e,e'pn) reactions, as well as from previous (p,2pn) data. The results and references are listed in table S1.

References and Notes

1. L. Lapikas, *Nucl. Phys. A.* **553**, 297 (1993).
2. J. Kelly, *Adv. Nucl. Phys.* **23**, 75 (1996).
3. W. H. Dickhoff, C. Barbieri, *Prog. Part. Nucl. Phys.* **52**, 377 (2004).
4. K. S. Egiyan *et al.*, *Phys. Rev. C Nucl. Phys.* **68**, 014313 (2003).

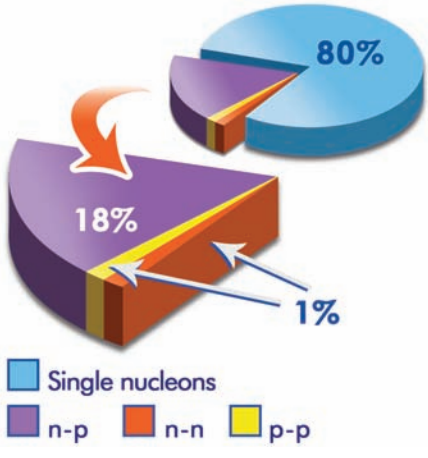

Fig. 3. The average fraction of nucleons in the various initial-state configurations of ^{12}C.

5. K. S. Egiyan *et al.*, *Phys. Rev. Lett.* **96**, 082501 (2006).
6. R. A. Niyazov *et al.*, *Phys. Rev. Lett.* **92**, 052303 (2004).
7. F. Benmokhtar *et al.*, *Phys. Rev. Lett.* **94**, 082305 (2005).
8. J. L. S. Aclander *et al.*, *Phys. Lett. B* **453**, 211 (1999).
9. A. Tang *et al.*, *Phys. Rev. Lett.* **90**, 042301 (2003).
10. A. Malki *et al.*, *Phys. Rev. C Nucl. Phys.* **65**, 015207 (2002).
11. E. Piasetzky, M. Sargsian, L. Frankfurt, M. Strikman, J. W. Watson, *Phys. Rev. Lett.* **97**, 162504 (2006).
12. R. Shneor *et al.*, *Phys. Rev. Lett.* **99**, 072501 (2007).
13. L. L. Frankfurt, M. I. Strikman, *Phys. Rep.* **76**, 215 (1981).
14. L. L. Frankfurt, M. I. Strikman, D. B. Day, M. Sargsian, *Phys. Rev. C Nucl. Phys.* **48**, 2451 (1993).
15. J. Alcorn *et al.*, *Nucl. Instrum. Methods* **A522**, 294 (2004).
16. Materials and methods are available as supporting material on *Science* Online.
17. I. Mardor, Y. Mardor, E. Piasetzky, J. Alster, M. M. Sargsian, *Phys. Rev. C Nucl. Phys.* **46**, 761 (1992).
18. R. Schiavilla, R. B. Wiringa, S. C. Pieper, J. Carlson, *Phys. Rev. Lett.* **98**, 132501 (2007).
19. M. M. Sargsian, T. V. Abrahamyan, M. I. Strikman, L. L. Frankfurt, *Phys. Rev. C Nucl. Phys.* **71**, 044615 (2005).
20. J. M. Lattimer, M. Prakash, *Science* **304**, 536 (2004).
21. G. Baym, *Nucl. Phys. A.* **590**, 233 (1995).
22. G. Baym, *Nucl. Phys. A.* **702**, 3 (2002).
23. T. Frick, H. Muther, A. Rios, A. Polls, A. Ramos, *Phys. Rev. C Nucl. Phys.* **71**, 014313 (2005).
24. This work was supported by the Israel Science Foundation, the U.S.-Israeli Binational Scientific Foundation, the UK Engineering and Physical Sciences Research Council and Science and Technology Facilities Council, NSF, and the U.S. Department of Energy (DOE) (grants DE-AC02-06CH11357 and DE-FG02-94ER40818 and U.S. DOE contract no. DE-AC05-84150, modification no. M175, under which the Southeastern Universities Research Association, Inc. operates the Thomas Jefferson National Accelerator Facility). The raw data from this experiment are archived in Jefferson Lab's mass storage silo.

Supporting Online Material

www.sciencemag.org/cgi/content/full/320/5882/1476/DC1
Materials and Methods
Figs. S1 and S2
Table S1
References

19 February 2008; accepted 8 May 2008
10.1126/science.1156675

Laser-Induced Electron Tunneling and Diffraction

M. Meckel,[1,2] D. Comtois,[3] D. Zeidler,[1,4] A. Staudte,[1,2] D. Pavičić,[1] H. C. Bandulet,[3] H. Pépin,[3] J. C. Kieffer,[3] R. Dörner,[2] D. M. Villeneuve,[1] P. B. Corkum[1]*

Molecular structure is usually determined by measuring the diffraction pattern the molecule impresses on x-rays or electrons. We used a laser field to extract electrons from the molecule itself, accelerate them, and in some cases force them to recollide with and diffract from the parent ion, all within a fraction of a laser period. Here, we show that the momentum distribution of the extracted electron carries the fingerprint of the highest occupied molecular orbital, whereas the elastically scattered electrons reveal the position of the nuclear components of the molecule. Thus, in one comprehensive technology, the photoelectrons give detailed information about the electronic orbital and the position of the nuclei.

Molecular multiphoton ionization in the tunneling limit (sketched in the upper frame of Fig. 1) is similar to tunneling in a scanning tunneling microscope (STM) (*1*). In both cases, electrons escape from the outer regions of the orbital to the continuum; that is, to the vacuum for multiphoton ionization of gas phase molecules or to the conduction band of the metal tip in a STM. In a STM, the sample is fixed and the tip is moved. Rotating the molecule with respect to the field direction is the analog of moving the tip. The resulting angle-dependent ionization probability (*2*–*5*) provides information for a molecule analogous to the position dependence of the tunneling current in a STM. However, whereas the total tunneling current is one observable, the electron wave packet that emerges into the vacuum from the tunnel retains more information about the orbital.

In contrast to the static field of a STM, the electric field in a laser pulse oscillates and forces a fraction of the tunneled electron wave packet back to the parent ion. There, the wave packet can diffract from the molecule (lower frame in Fig. 1). This phenomenon has been called laser-induced electron diffraction (LIED) (*6*) and relates to recent research on ultrafast electron diffraction, where a femtosecond electron bunch is created at a photocathode and accelerated in an electrostatic field onto a molecular (*7*) or solid state (*8*) target. In our case, the molecule serves as its own photocathode, whereas the laser provides the accelerating field. This situation produces extremely high current densities and attosecond timing (*9*).

We report the observation of molecular tunneling spectroscopy and LIED. We measured electrons produced from aligned O_2 and N_2, resolving their three-dimensional (3D) momentum distribution. Comparing experiment and theory, we show that, in the two dimensions perpendicular to the field direction, the momentum distribution for these direct electrons is determined by the highest occupied molecular orbital (HOMO), observed through the filter of the suppressed binding potential (Fig. 1) through which the electron tunnels. We also demonstrate LIED (*6*) and confirm its origin with a simulation. Selecting the wavelength of the recollision electron modifies the diffraction pattern. Thus, one set of measurements simultaneously identifies the orbital wave function of the molecule and the position of the atoms in the molecule.

Laser-induced tunneling and diffraction exploit different parts of the ionizing electron wave packet. The fraction of the electron wave packet that is created while the field strength increases within an optical half-cycle departs directly and irrevocably from its parent ion. Only tunneling stands between the orbital and the electron detector. The wave packet that is born while the field decreases returns to the ion where it can elastically scatter (diffract), inelastically scatter, or recombine to (interfere with) the orbital from which it was extracted (*10*). These three scattering processes offer different perspectives on the molecule.

Tunneling, the process underlying all, probes the electronic structure of the neutral molecule. The recombination radiation, known as high-harmonic radiation, also measures the orbital structure of the neutral molecule (*11*). However, because high-harmonic generation starts with tunneling and ends with interference, these processes must be disentangled before the techniques can be generalized to complex orbitals. In contrast, elastic and inelastic scattering occur at the molecular ion. Inelastic rescattering is closely related to field-free collision physics (*12*, *13*). It can cause multiple ionization and subsequently lead to Coulomb explosion of small molecules. The molecular structure can then be inferred from the momentum vectors of the correlated ionic fragments. Elastic scattering is also sensitive to the potential structure of the molecular ion. However, here the molecular structure is encoded in the diffracting electron wave packet, making this imaging technique scaleable to more complex molecules.

For electron diffraction to be observable, the de Broglie wavelength of the electron needs to be on the order of the dimensions of the molecule. Small diatomic molecules have a bond length of ≈1 Å [1.9 atomic units (au)]. To obtain this wavelength, an electron would need a kinetic energy of 150 eV, corresponding to a momentum of 3.3 au. Electrons that are accelerated in the laser field and recollide with the parent molecule can easily reach this range of kinetic energies (*10*).

We recorded the momentum of electrons arising from tunneling ionization of aligned O_2 and N_2, employing a Cold Target Recoil Ion Mo-

[1]National Research Council of Canada, 100 Sussex Drive, Ottawa, Ontario, Canada, K1A 0R6. [2]Institut für Kernphysik, Johann Wolfgang Goethe Universität, Max-von-Laue Straße 1, D-60438 Frankfurt, Germany. [3]Institut National de la Recherche Scientifique–Énergie, Matériaux et Télécommunication, 1650 boulevard Lionel-Boulet, Varennes, Québec, Canada, J3X 1S2. [4]Carl Zeiss SMT AG, Rudolf-Eber-Straße 2, 73447 Oberkochen, Germany.

*To whom correspondence should be addressed. E-mail: paul.corkum@nrc.ca